PLASMA PHYSICS AND PLASMA METHODS

UDC 532.5, 537.39 PACS: 68.03.Hj
EDN: DUFCPP

Effect of electrode immersion depth on the development of pre-breakdown currents in distilled water

V. A. Panov, A. S. Saveliev, Yu. M. Kulikov

This experimental and numerical study covers the velocity field in distilled water, occurring at the pre-breakdown stage when a voltage pulse is applied to a needle electrode at various immersion depths. The obtained results are analyzed in terms of the extremum (maximum) of the flow velocity achieved in the observation area in close proximity to the high-voltage electrode. Satisfactory ratio was obtained between the experimental and numerical dependencies of the velocity extremum over time and the calculations. It showed that the maximum value of velocity in the emerging current is achieved at later times with increasing immersion depth. Decreasing the immersion depth leads to the occurrence of an electric discharge when the high-voltage electrode loses contact with the water due to the stream occurring near it. The conducted study shows the further direction of development of the constructed physical and mathematical model.

Keywords: liquid; electrical breakdown; EHD flows.

DOI: 10.51368/1996-0948-2025-1-31-37

Introduction

The interaction of liquids with plasma generated by electric discharge is a promising area of research, both from a fundamental perspective and for numerous practical applications, which include the deposition of functional coatings [1, 2], surface treatment of materials [3, 4], synthesis of nanoparticles and fine powders [5, 6], plasma reactors [7, 8], and purification systems [9].

In many studies, the main plasma-forming medium is a one percent solution of sodium chloride in water. In particular, studies in [10, 11] investigated the parameters of plasma generated by a high-frequency discharge (with a frequency of $f = 13.56$ MHz) between a jet electrolytic electrode and a metal electrode: the chemical composition (including electron concentration) and thermodynamic properties (rotational and vibrational temperatures of hydroxyl radicals). For a similar electrolyte, experimental studies were conducted to

Vladislav A. Panov, Senior Staff Scientist, Candidate of Physical and Mathematical Sciences
E-mail: panovvladislav@gmail.com
Andrei S. Saveliev, Senior Staff Scientist, Candidate of Physical and Mathematical Sciences
Yury M. Kulikov, Senior Staff Scientist, Candidate of Physical and Mathematical Sciences
Joint Institute for High Temperatures of the Russian Academy of Sciences
Bd. 2, 13, Izhorskaya st., Moscow, 125412 Russia

Received December 20, 2024
Revised January 20, 2025
Accepted January 27, 2025
Scientific specialty code: 1.3.13

investigate a discharge with a liquid electrolyte cathode in [12] within a current range of 50–100 mA and an interelectrode distance of 3–4 mm. The occurrence of current pulsations was recorded, which were studied under the assumption of droplet transfer of matter and charges from an aqueous solution into the discharge plasma. Based on the analysis of current oscillograms, the sizes of the resulting drops were estimated. The influence of the bubble structure on the nature of current and voltage pulsations in the discharge was studied in [13]. The authors presented results of experimental studies of an alternating current electric discharge at industrial frequency in a gas-liquid electrolyte medium with bubbles for interelectrode distances of 50–150 mm inside a dielectric tube. Based on the analysis of experimental data, the authors proposed a mechanism for the development of an alternating current electric discharge in a medium with microbubbles.

Experimental studies of alternating current discharge [14] of industrial frequency in a gas-liquid medium made it possible to determine a qualitative mechanism for the development of breakdown and discharge at low pressures. It was found that a gas-liquid medium, saturated with small gas bubbles ranging in size from 1 to 3 mm is formed with a decrease in pressure as a result of boiling and electrolysis. This, in turn, results in a breakdown and rapid ignition of a discharge in the porous medium near the solid electrode. The transition of an electrical discharge with microdischarges into a volumetric discharge at reduced pressures has been established.

Paper [15] proposes a physical mechanism for the formation of ring-shaped and semi-ring-shaped plasma structures around an electrolyte jet in a high-frequency discharge with liquid jet electrodes. It is shown that the electric field strength in the region of jet stream decay can reach values of 1–10 MV/m, at which field emission is possible, leading to the appearance of primary electrons in the vicinity of the jet, which leads to ionization and excitation of molecules of the surrounding gas environment.

In [16], it was determined that the effect of an atmospheric-pressure glow discharge on water results in the formation of hydrated electrons, the generation rate of which increases with the discharge current, while the energy yield remains constant at 0.13 ± 0.01 particles per 100 eV. Using the acceptor method, the generation rates and energy yields of hydrated electrons in water under the influence of an atmospheric pressure glow discharge were found.

Paper [17, 18] contains measurements of the electrical and spectral characteristics of a discharge with a liquid electrolyte cathode at atmospheric pressure in air within a current range of 20–90 mA. The dependences of the field strength on the magnitude of the discharge current were found for aqueous solutions with different compositions and different pH values, but with the same specific electrical conductivity of 300 μS/cm. It was found that the measured intensity of the glow of the second positive nitrogen system near the surface of the solution in the discharge for solutions with different compositions, different pH values, and electrical conductivity decreases with an increase in the discharge current in the current range from 20 to 100 mA. The rotational and vibrational temperatures determined for molecular nitrogen are the same for all experiments and are 2400 and 3800 K, respectively.

An analysis of the completed work shows that the main attention of researchers is focused on the electrophysical and spectral characteristics of discharges, while pre-breakdown electrohydrodynamic effects have received much less attention. The development of an electrical breakdown is possible not only as a result of a change in the physical and chemical properties of the stationary environment in which it develops, but also in combination with the phenomena

of its transfer and redistribution in the space near the electrodes. The consequence of such a phenomenon may be abnormally low breakdown voltage values [19, 20].

The aim of this work is an experimental and numerical study of the velocity field in distilled water that occurs when a voltage pulse is applied to the needle electrode at different immersion depths. The obtained results are analyzed in terms of the extremum (maximum) of the flow velocity achieved in the observation area in close proximity to the high-voltage electrode.

Experimental setup

In this study, the experimental unit used was described in detail in [21, 22], so only the main parameters are presented here. A cylindrical metal electrode with a diameter of $d = 0.85$ mm was immersed at different depths in distilled water contained in an optically transparent cube-shaped container with an edge of 8 cm. Using a high-voltage circuit, a pulse with an amplitude of 10 kV was applied to the electrode, causing current to flow through the water, with a rise time of about 100 ns and a duration of less than 1 ms. This caused the formation of a non-stationary liquid flow near the electrode surface. Using the Particle Image Velocimetry (PIV) method, the distribution of two components of the velocity vector of this flow in the plane of the electrode axis was determined. Measurements were carried out for four values of immersion depth h: 1d, 2d, 4d, 8d.

Numerical modeling

Numerical modeling of this problem requires the joint solution of equations belonging to different sections of physics. This circumstance imposes additional requirements on the calculations, namely: the use of a small-time step, splitting into physical processes, and the use of iterative solvers (Newton's methods with relaxation). The finite element method was used for spatial discretization. Electrostatic effects were described using the equation for electric potential:

$$\nabla \times \vec{D} = \rho_v, \ \vec{E} = -\nabla V, \ \vec{D} = \varepsilon E, \tag{1}$$

Where ρ_v is the volume density of electric charges, $\vec{D}$ is the electric induction vector, V is the electric potential, $\vec{E}$ is the electric field strength, and ε is the relative penetrability. In the problem under consideration, in addition to bound charges, there are also free charges (anions and cations of water formed during the equilibrium electrolytic dissociation process). To calculate the movement of ions, equations for concentration were solved:

$$\frac{\partial c_i}{\partial t} + \nabla \times \left(\vec{j} + \vec{u} c_i \right) = 0, \tag{2}$$

$$\vec{J} = -D_i \nabla c_i - z_i u_{m,i} F c_i \nabla V, \tag{3}$$

c_i is concentration of a certain type of particles, $\vec{j}$ is particle flow associated with concentration diffusion of ions and their drift in an electric field, $\vec{u}$ is convective transfer into a liquid flow, D_i is diffusion coefficient, z_i is ion charge, and F is Faraday number. The distribution of free and bound charges determines the volumetric force $\vec{F}_{es}$ acting on the liquid.

$$\vec{F}_{es} = \nabla \times \mathbf{T} + \rho_v \vec{E}, \tag{4}$$

$$T_{ij} = -\frac{\varepsilon \varepsilon_0 E^2}{2} \delta_{ij} + \varepsilon \varepsilon_0 E_i E_j \tag{5}$$

where $\mathbf{T}$ is the Maxwell stress tensor, ε_0 is the penetrability of vacuum, and δ_{ij} is the symbol for the Kronecker tensor.

The value of the electrostatic force allows us to find the distribution of velocity

and pressure based on the equations of motion of a viscous incompressible medium

$$\rho\frac{\partial\vec{u}}{\partial t}+\rho\left(\vec{u}\times\nabla\right)\vec{u}=\nabla\times\left[-p\mathbf{I}+\mathbf{K}\right]+\vec{F}_{es} \qquad (6)$$

$$\frac{\partial\rho}{\partial t}+\nabla\times\left(\rho\vec{u}\right)=0, \qquad (7)$$

which are supplemented by relations for the barotropic fluid $\rho(p)=\frac{p}{c^2}+\rho_0$, of the stress tensor $\mathbf{K}=\mu\left(\nabla\vec{u}+\left(\nabla\vec{u}\right)^T\right)-\frac{2}{3}\mu\left(\nabla\times\vec{u}\right)\mathbf{I}$.

Splitting by physical processes leads to the following algorithm for calculating unknowns at the new time layer: (1) – the speed and pressure are found using the known electric field and charge distribution, (2) – the concentration of positive ions is calculated, (3) – the concentration of negative ions is found. Based on the new velocity field and the distribution of free charges, a new distribution of the electric field is determined (4).

For time iteration, an implicit method with second order approximation and variable step is used. To find a solution to a linearized system of equations, Newton's method is used. For each group of unknowns, the parameters of the Newton method are adjusted individually to ensure accelerated convergence.

Results and discussion

Experiments and calculations were carried out at the same values of the electrode immersion depth (h = 1d, 2d, 4d, 8d).

Figure 1 shows the dependence of the maximum average velocity in the observed region, normalized to the value at late times of the flow. It is evident that the velocity recorded in the experiment (curves 1 and 3) in the initial interval of flow development up to 30 μs significantly exceeds the values obtained as a result of numerical modeling (curves 2 and 4). One of the reasons for the differences may be the influence of the moving interphase boundary (water-air), while in the calculation the interface surface of the media is fixed. The significant discrepancy at the initial moment of time may probably also be a consequence of the fact that the PIV method has difficulty measuring the velocity in a small vicinity of the electrode due to the relatively small number of particles in this region. When the electrode was immersed to a depth of $h = d$ at times exceeding 256 μs after the start of the current pulse, a drop in the water level below the electrode was observed, which led to the formation of an air gap between them and a spark discharge, which significantly altered the flow pattern near the electrode. A similar effect was observed at longer time values during immersion to a depth of h = 2–4d. In this regard, time measurements are limited to 1 μs.

With an increase in the immersion depth to $h = 2d$ (see Fig. 1, curves 3 and 4), satisfactory agreement between the curves is observed at late calculation times. A distinctive feature of curve (2) is the velocity oscillations, which are caused by the existence of large-scale vortices propagating downwards through the computational domain. These vortices are one of the features of the axially symmetric model, since in the experiment, when moving away from the rod, a three-dimensional evolution of these structures is observed (leading to the disintegration of vortices into smaller ones).

Figure 2 shows an instantaneous picture of water flow near the electrode at a time of 256 μs. The axis $x = 0$ coincides with the axis of the electrode, and the straight line y = 46.5 mm coincides with its edge. The color shows the modulus of the velocity vector normalized to the maximum flow velocity, which is achieved at later times, and the arrows show the direction of fluid movement. It is evident that the flow in the

near-electrode region at the end of the rod is vortex, and, due to the presence of some arbitrary vorticity field in the liquid, as well as the non-uniformity of the distribution of the electric potential in the vicinity of the end of the rod, it is three-dimensional.

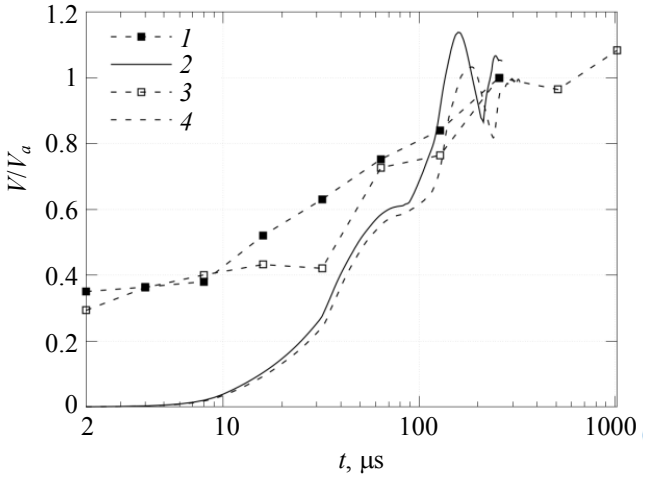

Fig. 1. Reduced maximum flow velocity at rod immersion depth h = 1d: experiment (1) and modeling (2), and depth h = 2d: experiment (3) and modeling (4)

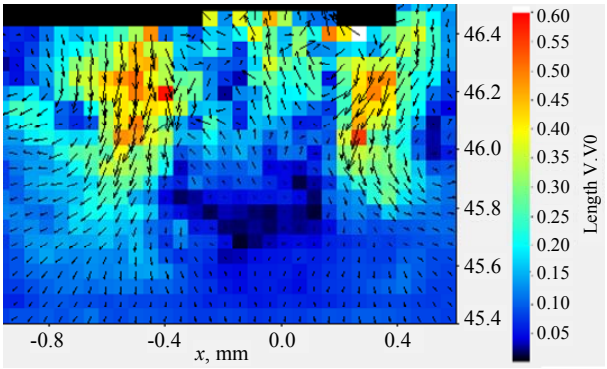

Fig. 2. Velocity field near the needle surface at 256 μs after the current pulse is applied

The best agreement between the modeling results and the experiment in the vicinity of $t = 100$ μs is observed for the case of $h = 4d$ (Fig. 3), while the calculated curve of the reduced velocity similarly experiences oscillations. For the case of $h = 8d$, the reduced velocity obtained in the calculation exceeds the experimental result.

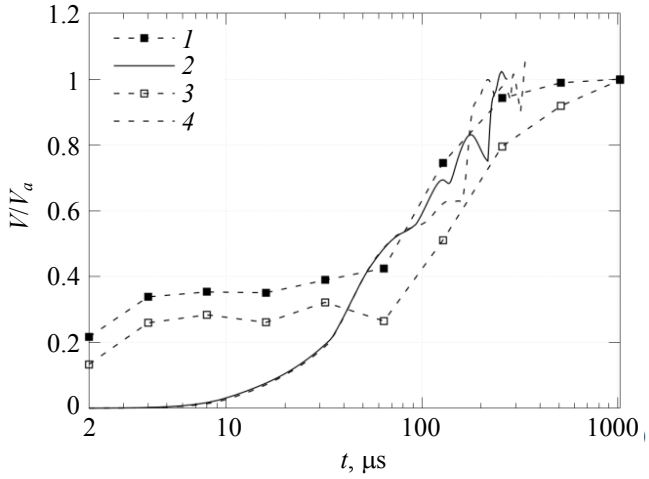

Fig. 3. Reduced maximum flow velocity at rod immersion depth h = 4d: experiment (1) and simulation (2), and depth h = 8d: experiment (3) and simulation (4)

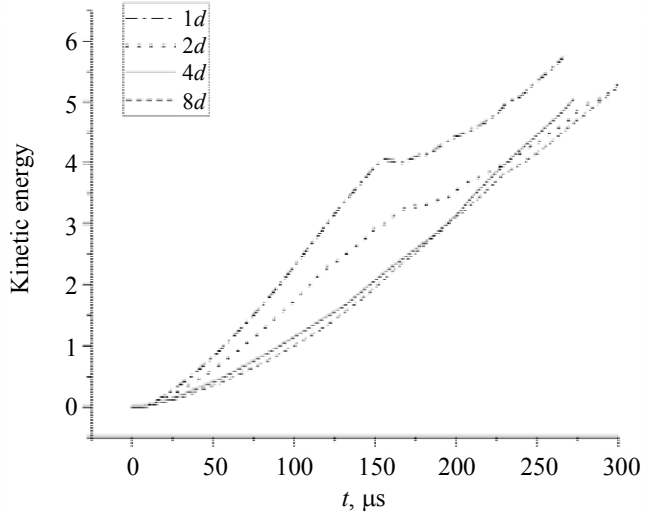

Fig. 4. Dependence of the reduced kinetic energy of the flow on time at different rod immersion depths. Processing of modeling results

The experimental results were obtained in the vicinity of the electrode, which makes it difficult to introduce integral quantities often considered in theory. Therefore, the behavior of kinetic energy, one of the integrals of the system, is considered based on the results of numerical modeling. Figure 4 shows the values of kinetic energy reduced to the value for $h = 8d$ at $t = 100$ μs (the end of the interval of regular behavior of the curves). It is evident that increasing the depth

of immersion of the rod leads to a decrease in the kinetic energy of the system. This can be explained as follows. A shallow immersion depth leads to a higher concentration of the electric field around the electrode tip, and thus to a greater electrostatic force acting on an elementary volume of liquid, resulting in a faster acceleration of the fluid. In this case, the maximum value of velocity in the emerging current is achieved at later times with increasing immersion depth.

Conclusion

An important role in the process of movement of the horizontal interphase boundary in the vertical electric field is played by disturbances in the water, propagating at the speed of sound when voltage is applied. These disturbances deform the water-air interface, which leads to the emergence of a large-scale flow directed from the bottom up along the rod. This experimental fact requires considering the mobility of this boundary and the effects of surface tension. The double layer that forms around the metal electrode even before voltage is applied requires special attention. This layer results in small-scale (on the order of 100 nm) and highly significant (40–45 times) non-uniformity in the dielectric penetrability of water, which imposes additional requirements on the grid resolution of the near-electrode zone. Applying voltage to the electrode leads to charge separation in the near-electrode region and its deprotonation, and also activates a number of nonlinear effects in areas of particularly strong electric fields on the sharp edges of the electrode, which are characteristic of polar liquids in general and water in particular, non-equilibrium electrolytic dissociation of water, and non-linear transport of protons. In addition, it is very difficult to consider the penetration of atoms and microscopic fragments of the electrode into the near-electrode layers of the liquid.

The model proposed in the study is essentially non-linear both in space (in the near-electrode layer) and in time and forms a system with positive feedback: applying a high-voltage potential to the electrode needle results in an increase of the ion concentration (by several orders of magnitude during the calculation time) and shielding. Shielding, in turn, results in an increase in the electric field and its gradients, and, ultimately, to an increase in the amplitude of the volume force acting on the liquid. However, in order to break this connection, as well as to consider the propagation of disturbances along the boundary, it is recommended to further develop a special “near-electrode” model of a compressible continuous medium that correctly considers the various nonlinearities listed.

REFERENCES

1. Paulmier T., Bell J. M. and Fredericks P. M., Thin Solid Films **515**, 2926 (2007).

2. Quan C. and He Y., Surf. Coat **269**, 319 (2015).

3. Meletis E. I., Nie X., Wang F. L. and Jiang J. C., Surf. Coat. Technol. **150**, 246 (2002).

4. Ishijima T., Nosaka K., Tanaka Y., Uesugi Y., Goto Y. and Horibe H., Appl. Phys. Lett. **103**, 142101 (2013).
https://doi.org/10.1063/1.4823530

5. Wüthrich R. and Allagui A., Electrochim. Acta **55**, 8189 (2010).

6. Abdul K. T. and Kaliani A., Ionics **18**, 315 (2012).

7. Becker K. H., Schoenbach K. H. and Eden J. G., J. Phys. D: Appl. Phys. **39**, R55 (2006).

8. Gao S. Z., Ma D., Lu Q., Li Y., Li X. and Yang W., Plasma Chem. Plasma Process. **30**, 873 (2010).

9. Son E. E., Sadriev R. Sh., Gaisin Al. F., Bagautdinova L. N., Gaisin F. M., Shakirova E. F., Akhatov M. F., Gaisin Az. F. and Kayumov R. R., High Temperature **52**, 939 (2014).

10. Gaisin A. F., Gaisin F. M., Zheltukhin V. S. et al., Plasma Phys. Rep. **48**, 48 (2022).

11. Kayumov R. R., Kuputdinova A. I., Mirkhanov D. N. et al., Plasma Phys. Rep. **50**, 115 (2024).

12. Tazmeev G. K., Tazmeev A. K. and Tazmeev K. K., Applied Physics, No. 3, 33 (2023) [in Russian].

13. Valiev R. I., Khafizov A. A., Bagautdinova L. N. et al., High. Temp. **60**, Suppl. 1, 127–130 (2022).

14. Khafizov A. A., Valieva R. I., Bagautdinova L. N., Gaisin Az. F., Gaisin Al. F., Gaisin F. M., Sond E. E. and Fakhrutdinova I. T., High Temp. **60** (4), 570 (2022).

15. Zheltukhin V. S., Gaisin A. F. and Petryakov S. Y., Technical Physics Letters, No. 9, 22 (2022).

16. Khlyustova A. V. and Titov V. A., Applied Physics, No. 6, 48 (2015) [in Russian].

17. Chistolinov A. V., Tyuftyaev A. S. and Gadzhiev M. Kh., Applied Physics, No. 5, 5 (2021) [in Russian].

18. Chistolinov A. V., Yakushin R. V. and Perfilieva A. V., Applied Physics, No. 1, 12 (2022).

19. Panov V. A., Kulikov Yu. M., Pecherkin V. Ya., Vasilyak L. M. and Saveliev A. S., Applied Physics, No. 6, 5 (2023) [in Russian].

20. Panov V. A., Kulikov Yu. M., Vetchinin S. P., Pecherkin V. Ya. and Vasilyak L. M., Plasma Sources Sci. Technol. **32** (9), 095020 (2023).

21. Panov V. A., Saveliev A. S., Pecherkin V. Ya., Vasilyak L. M. and Kulikov Yu. M., Journal of Communications Technology and Electronics **68**, Suppl. 2, 170–175 (2023).

22. Panov V. A., Saveliev A. S. and Kulikov Yu. M., Applied Physics, No. 4, 89 (2024) [in Russian].